Short ranged attraction and long ranged repulsion between two solute particles in a subcritical liquid solvent

2006 J. Phys.: Condens. Matter 18 L81

(http://iopscience.iop.org/0953-8984/18/6/L01)

INSTITUTE OF PHYSICS PUBLISHING JOURNAL OF PHYSICS: CONDENSED MATTER

J. Phys.: Condens. Matter **18** (2006) L81–L87 doi:10.1088/0953-8984/18/6/L01

LETTER TO THE EDITOR

Short ranged attraction and long ranged repulsion between two solute particles in a subcritical liquid solvent

J Chakrabarti[1], **S Chakrabarti**[2] **and H Löwen**[3]

[1] S N Bose National Centre for Basic Sciences, Block-JD, Sector-III, Salt Lake, Calcutta-700091, India
[2] Department of Physics, Krishnagar Government College, Krishnanagar, West Bengal-741101, India
[3] Institut für Theoretische Physik II, Heinrich-Heine-Universität Düsseldorf, Universitätsstraße 1, D-40225 Düsseldorf, Germany

Received 11 November 2005, in final form 8 January 2006
Published 24 January 2006
Online at stacks.iop.org/JPhysCM/18/L81

Abstract

We calculate the effective interaction between two solute particles in a solvent of Lennard-Jones (LJ) particles in two dimensions where the solvent is in the stable liquid phase near the liquid–gas phase coexistence and the solute–solvent interaction is repulsive. Our grand canonical Monte Carlo (GCMC) simulations show that the effective interaction between two solute particles is attractive for separations between the solute particles up to a range of a few nanometres, beyond which the interaction exhibits a marked repulsion. Such an effective interaction stabilizes clusters of nanometre (nm) sizes.

A fluid solvent close to its critical point has drawn recent interests due to potential industrial applications. Supercritical solvents, known as 'Green Chemistry' solvents, are used for environment friendly waste processing [1]. Subcritical liquid water is extensively used in the extraction processes in agricultural industries [2]. Other solvents close to phase transitions include, for instance, a solvent mixture close to a fluid–fluid demixing transition [3], and a liquid crystalline solvent close to its isotropic nematic transition [4]. The key issue in these applications is how the solute particles are solvated [5] via the redistribution of the solvent particles around the solute. The solvent mediated effective force between two solute surfaces is crucial to industrial applications and interesting pedagogically, as the effective force determines the structure and dynamics of the solute in the solution [6]. If a solvent below its phase-coexistence is placed in contact with a surface, and the solute surface prefers the unstable phase relative to the stable solvent phase, the surface gets wetted, namely, covered by the unstable solvent phase, the other part of the solvent remaining in the stable bulk phase. For instance, if the solvent is in the stable bulk gas phase below the bulk liquid–gas phase coexistence, and the solute surface is 'solvophilic', namely, having attractive solute–solvent interactions, the surface is wetted by liquid layers. The solvent mediated effective wall–particle force in solvophilic

condition exhibits anomalies at a separation where the two liquid layers bridge [7–9]. On the other hand, if the solvent is in the bulk *subcritical liquid* phase below the gas–liquid phase coexistence, and the solute surface is 'solvophobic', namely, having a repulsive solute–solvent interaction, the solute surface gets covered by the gas phase. Reference [10] deals with both solvophobic and solvophilic walls with respect to a particular component, immersed in a binary mixture in the two-phase region. This work shows that the solvation force is attractive for solvophobic walls and oscillatory for solvophilic ones. It is important to note that the wetting behaviour depends crucially on the geometry of the surface [11]. While an infinite planar surface could be completely wetted by the unstable phase with a diverging thickness, a surface with a finite curvature can have only partial wetting, the thickness of the layer of the unstable phase being large but finite. A natural question arises: Does the partial wetting affect the solvent mediated effective force between a pair of solute particles? Earlier works [7–10] do not address this issue. Reference [12] deals with effective interaction between two dry spheres in water, albeit far from the solvent phase transition.

With this backdrop we report our simulation studies in two dimensions on the effective force between two solvophobic circular solute particles mimicking the finite curvature effects, the solvent being an LJ system in the stable subcritical liquid phase below the bulk gas–liquid coexistence. Our GCMC simulations show an attractive effective force between two solute particles for smaller separations whose range, determined by the thickness l_b of the gaseous solvent interface around the solute particle, extends up to a few nanometres. More interestingly, the consequence of having a finite thickness of the solvent density profile around a spherical solute particle follows for separations larger than $2l_b$. The bulk solvent liquid now fills up the intervening region between the solutes, leading to a weak and longer ranged repulsive force unlike that described in [10]. We further show by Monte Carlo (MC) simulations that such an effective interaction leads to cluster formation of the solutes. Our work theoretically demonstrates in a system the presence of a short ranged attraction and long ranged repulsion which has been proposed recently to explain cluster formation in a wide range of systems of technological as well as biological interest [13, 14].

We simulate a bulk two-dimensional (2D) LJ solvent at $\epsilon/k_{\mathrm{B}}T = 0.45$ [15] by the standard GCMC techniques [16] at a given chemical potential $\mu/k_{\mathrm{B}}T$ in a periodic $50\sigma \times 50\sigma$ box, σ being the LJ length parameter. The bulk $\rho_0^*(=\rho_0\sigma^2$, ρ_0 being the number density) versus $\mu/k_{\mathrm{B}}T$ data, shown in figure 1(a), indicates a jump at $\mu/k_{\mathrm{B}}T = -3.8$ with the coexisting liquid density (=0.72) and gas density (=0.04) in agreement with the known data [15]. Next we carry out the GCMC simulations with a single solute sphere in the solvent for $\mu/k_{\mathrm{B}}T$ in a subcritical liquid phase. The solvophobic solvent–solute interaction has a hard-core of radius r_{c} and a softer tail: $V_{\mathrm{ss}}(|\vec{r} - \vec{R}|) = \epsilon_{\mathrm{ss}}[\sigma_{\mathrm{ss}}/(|\vec{r} - \vec{R}| - r_{\mathrm{c}})]^{12}$, the solvent being at $\vec{r}$, the solute at $\vec{R}$, ϵ_{ss} being the scale of the softer repulsive interaction and σ_{ss} its range. We take $\epsilon_{\mathrm{ss}}/\epsilon = 5$, $\sigma_{\mathrm{ss}}/\sigma = 1$ and $r_{\mathrm{c}} = 2.5\sigma$. The solvent density profile, $\rho^*(s) = \rho(s)\sigma^2$, s being $|\vec{r} - \vec{R}|/\sigma$, about the solute at $\vec{R} = 0$ has been shown in the inset of figure 1(a) for different $\mu/k_{\mathrm{B}}T$. $\rho^*(s)$ is significantly lower than the bulk ρ_0^* in the vicinity of the solute. $\rho_{\mathrm{s}}^* \to \rho_0^*$ over an interfacial width l_b^* $(=l_b/\sigma$, l_b being the length of the interfacial region). Note that $l_b^* \sim 7.5$, significantly larger than r_{c}/σ at $\mu/k_{\mathrm{B}}T = -3.7$, and decreases as $\mu/k_{\mathrm{B}}T$ moves away from the coexistence.

Finally we perform GCMC simulations by inserting a pair of solute particles at $\vec{R}_1/\sigma = (s_{12}/2, 0)$ and $\vec{R}_2/\sigma = (-s_{12}/2, 0)$ along the x-axis. Insets I and II in figure 1(b) show two snapshots of equilibrated configurations (50 000 GCMC steps) of the solvent particles for $s_{12} = 12$ and 16 respectively. While $s_{12} = 12$ shows clear depletion of the solvent particles between the solutes, the solvent configuration for $s_{12} = 16$ consists of two vapour bubbles with the solute particles at the core, submerged in the liquid phase. Due to the finite

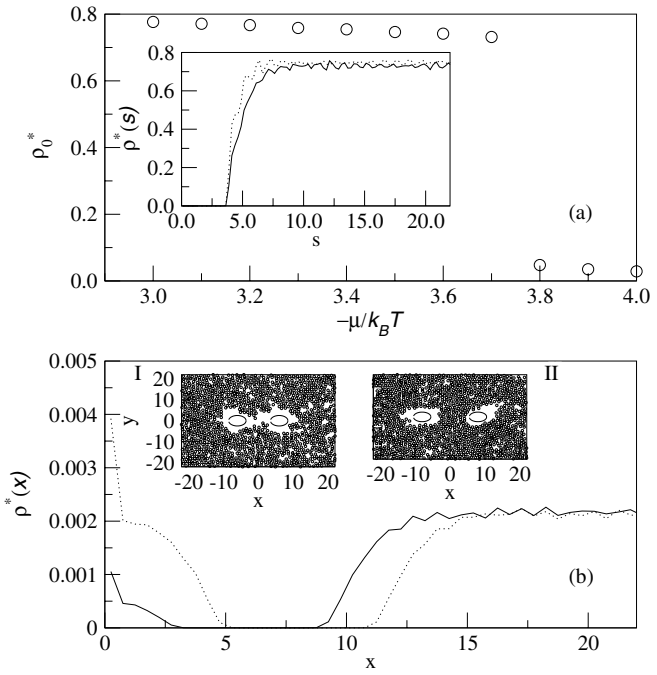

Figure 1. Data from different GCMC simulations. (a) The bulk density ρ_0^* versus $-\mu/k_BT$ plot for the 2D LJ solvent at $\epsilon/k_BT = 0.45$ without any solute particle. The discontinuity in ρ_0^* values (0.04 and 0.7) around $\mu/k_BT = -3.8$ is taken to be the gas–liquid coexistence. Inset: the solvent density profile $\rho^*(s)$ as a function of s, the distance from the centre of a solvophobic solute fixed at the centre of the simulation box for $\mu/k_BT = -3.7$ (the solid line) and -3.5 (the dotted line). (b) The density of solvent particles lying within $2r_c = 5.0$ distance around the axis (x-axis) joining a pair of solvophobic solute placed symmetrically about the centre of the box, $\rho^*(x)$, as a function of x, the distance from the centre of the box, at $\mu/k_BT = -3.7$ for different distances s_{12} between the solute pair: $s_{12} = 12$ (solid line) and $s_{12} = 16$ (dotted line). Only the positive half of the x-axis has been shown due to the inversion symmetry. Equilibrated configuration snapshot at $\mu/k_BT = -3.7$ for $s_{12} = 12$ (inset I) and $s_{12} = 16$ (inset II). The circles show the solute particles.

thickness of the drying layer around the finite-sized solute, the stable liquid phase occupies the intervening region between the solutes. The density profiles, averaged over 1000 equilibrium configurations, along the x-axis, $\rho^*(x) = \rho(x)\sigma^2$, of the solvent particles within a rectangular strip of size $2r_c$, chosen symmetrically about the x-axis, have been shown in figure 1(b) for $\mu/k_BT = -3.7$ for different s_{12}. The centre of the box, $x = 0$, is significantly depleted of solvent particles, compared to the large-x region at $s_{12} = 12.0$. This behaviour persists up to $s_{12} \simeq 2l_b^*$. However, the solvent density at $x = 0$ at $s_{12} = 16.0$ is higher compared to that surrounding the solutes. The higher $\rho(x)$ at $x = 0$ is a consequence of presence of the two confining gas–liquid interfaces.

We calculate the solvent mediated average effective force between the two solute particles, given by [6]: $\langle f^*(s_{12})\rangle = \langle f(s_{12})\sigma/k_BT\rangle = \frac{1}{2k_BT}\frac{(\vec{R}_1-\vec{R}_2)}{|\vec{R}_1-\vec{R}_2|}\langle\sum_i[\frac{\partial}{\partial\vec{R}_1}V_{ss}(|\vec{r}_i-\vec{R}_1|)+\frac{\partial}{\partial\vec{R}_2}V_{ss}(|\vec{r}_i-\vec{R}_2|)]\rangle$, $\vec{r}_i$ being the position of the ith solvent particle and $\langle\cdots\rangle$ a grand canonical average over 50 000 configurations. The $\langle f^*(s_{12})\rangle$ versus s_{12} data has been shown in figure 2(a) for $\mu/k_BT = -3.7$. The force is attractive up to $s_{12} \sim 2l_b^*$. Physically, the osmotic pressure imbalance, created by the higher solvent particle density around the two solute particles compared to that in the intervening region (inset I, figure 1(b)), leads to an effective attraction

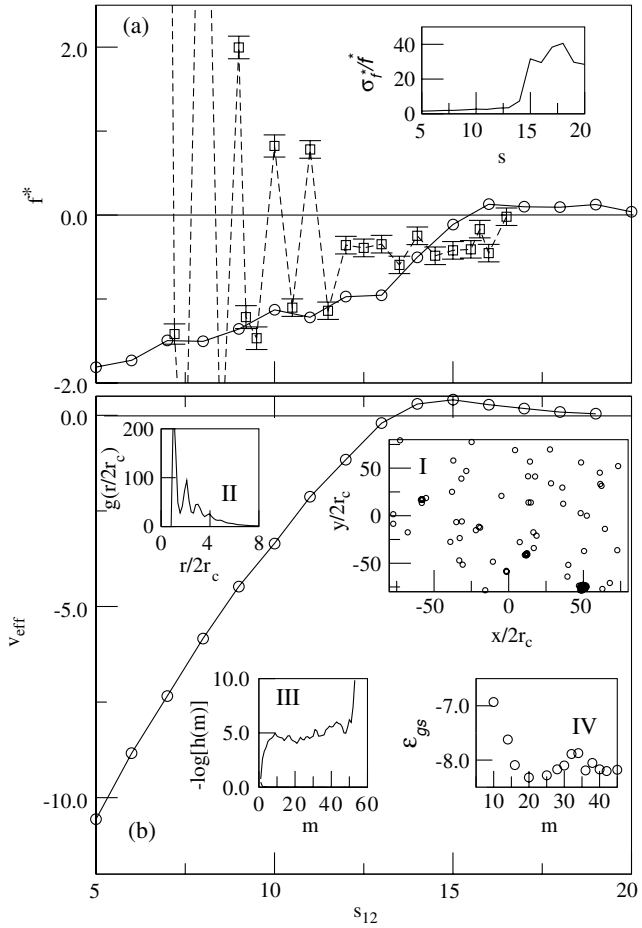

Figure 2. (a) Effective force, $\langle f^*(s_{12})\rangle$, as a function of s_{12} in different cases: $\mu/k_{\rm B}T = -3.7$ (circles) and $\mu/k_{\rm B}T = -3.9$ (squares with error bars). The solid and the dashed lines are guides to the eyes. The error in the first case (circles), being 1–2%, is too small to be shown in the scale of the y-axis. Note here that $\langle f^*(s_{12})\rangle$ is attractive for $s_{12} \simeq 2l_b$, beyond which it becomes repulsive. Further, note the qualitative difference of $\langle f^*(s_{12})\rangle$ in the two cases. Inset: the fluctuations of force, $\sigma_{f^*(s_{12})}/\langle f^*(s_{12})\rangle$, as a function of s_{12} for $\mu/k_{\rm B}T = -3.7$. (b) Effective potential, $U(s_{12})$, as a function of s_{12} for $\mu/k_{\rm B}T = -3.7$. Inset I: an equilibrated snapshot of MC simulations on the solute particles alone with the effective pair potential as in (b) with a hard core at $2r_{\rm c}$. The clustered patches of finite size are clear. Inset II: $g(r/2r_{\rm c})$ versus $r/2r_{\rm c}$ plot. The peaks indicate a typical cluster size of $\sim 7r_{\rm c}$. Inset III: the probability distribution $h(m)$ of finding a cluster with m particles as a function of m in log-normal plot. Inset IV: the ground state energy $\epsilon_{\rm gs}$ for different m number of particles in a closed box with the same area as a typical cluster. Note that the horizontal axis of (a), not marked separately, is s_{12} and scaled as in that of (b).

between the solute particles up to $s_{12} \sim 2l_b^*$. This large range is in marked contrast to that in depletion mediated attraction, which is, for instance, realized in hard sphere solutes and solvents [17] where it is only of the order of the solvent hard core. Moreover, here the interfacial width of the solvent distribution around the solute determines the range of attraction, and is observed to be sensitive to the proximity to the phase coexistence.

$\langle f^*(s_{12})\rangle$ changes over to repulsion for $s_{12} > 2l_b^*$. This is a consequence of the finite thickness of the drying layers around the finite solutes. Inset II in figure 1(b) shows a stable

liquid phase in the region between the solutes. The liquid surrounding a vapour bubble exerts inward pressure on the interface of the bubble which exceeds the outward pressure exerted on the interface by the gas, the pressure gradient being counterbalanced by the interfacial surface tension according to the classical Laplace formula, to provide stability to the gas bubbles surrounding the solute particle core. The local density of the liquid being larger in between the particles than that in the surrounding region as in figure 1(b), the bubbles are pushed away from each other. More quantitatively, the repulsion induced via the liquid layer intervening between the gas bubbles comes from a repellant effective interface potential between two liquid–gas interfaces [11]. Our repulsion data show an exponential decay with length scale of about 3σ, comparable to the correlation length in the bulk liquid [11]. Therefore, the range of the repulsion can be tuned via the location of liquid–gas solvent coexistence in the bulk phase diagram which is relevant for equilibrium cluster formation [18]. The repulsive $\langle f^*(s_{12})\rangle$ for large s_{12} is in sharp contrast to the findings in [10] with hydrophobic plates. Here the wetting layer thickness diverges, excluding the possibility of repulsion induced via intervening stable bulk phase. Our data thus bring out the important role of the curvature in determining the effective interaction. We also point out the qualitative difference of our observations from the long ranged attractive solvation pressure, falling off as slowly as $-1/h^3$, between a pair of plates induced via capillary drying [19, 20] where, unlike our case, the bulk fluid solvent is not close to phase transition. However, reference [21] by simulating model water shows that metastable liquid water exists between two slits even when capillary drying is expected, resulting in repulsion down to very small separations.

The fluctuations of the force, $\sigma_{f^*(s_{12})}/\langle f^*(s_{12})\rangle$, $\sigma_{f^*(s_{12})}$ being the standard deviation of the force sampled over the equilibrium configurations, are shown as a function of s_{12} in the inset of figure 2(a) for $\mu/k_BT = -3.7$. There are enormous fluctuations at bridging of the drying layers around $s_{12} = 2l_b^*$, indicating that the mean field theories [8] may not be applicable to the present scenario.

We show in figure 2(a) for comparison the $\langle f^*(s_{12})\rangle$ data in the subcritical vapour solvent condition, $\mu/k_BT = -3.9$, with solvophilic solute–solvent interaction where thick liquid layers grow around the solute. $\langle f^*(s_{12})\rangle$ decays to zero around $s_{12} \approx 17$. With decreasing s_{12}, we find an attractive effective force at $s_{12} \approx 16.0$, where the liquid layers on the two solutes start to overlap. Then, the force stays almost *constant* so long as the bridge remains intact, as in [8], down to $s_{12} \approx 13.0$. In sharp contrast to the metastable gas bubbles, the metastable liquid droplets attract each other. The effective interface potential repulsion is drastically reduced in the opposite case of a stable gas phase: here, there is no large correlation length for a gas layer between two liquid droplets such that this force is masked by attractive interface fluctuations. $\langle f^*(s_{12})\rangle$ is oscillatory below $s_{12} \approx 13$ due to liquid layer correlations.

The effective potential, $U(s_{12})$, is obtained by integrating the force data for $\mu/k_BT = -3.7$. $U(s_{12})$, shown in figure 2(b), has an attractive well of depth of $-10k_BT$ and a range of $2l_b$, beyond which it is weakly repulsive, having a potential barrier $\sim k_BT$. Such a deep attraction can lead to aggregation of the solute particles, surrounded by the gas bubbles. However, the repulsion beyond $2l_b$ would prevent flocculation of the solute aggregates, leading to clusters of equilibrium size of $2l_b\sim$ a few nanometres. We verify this scenario by performing MC simulations on a system of 100 solute particles in a square periodic box having solute volume fraction 0.003 with a pair interaction potential as in figure 2(b), superimposed on a hard core diameter of $2r_c$. Inset I in figure 2(b) shows an equilibrium configuration snapshot having finite clusters. Inset II of figure 2(b) shows the pair distribution function, $g(r)$, namely, the probability of finding a pair of particles at separation r [16]. $g(r)$ has strong peaks up to $r/2r_c \simeq 3.5$, indicating typical cluster diameter $\sim 7r_c$, quite comparable to $2l_b$. The probability distribution $h(m)$, to find a cluster of m particles [16], has been plotted in inset III of figure 2(b)

which shows that clusters having $m \simeq 20$ particles are the most prevalent ones, apart from the usual single particle peak. In order to ensure that the condensation in the clusters takes place up to a finite m, we consider a closed box of area equal to that of a typical cluster and calculate the ground state energy [13] ϵ_{gs} for different m. Any non-trivial minimum of ϵ_{gs} gives the maximum number of particles in a cluster, for the entropy effects would tend to reduce the clusters to smaller sizes. ϵ_{gs}, shown in inset IV of figure 2(b), has a minimum around $m = 20$ which is consistent with the dominant cluster size[4].

In conclusion we show that two solvophobic solute particles in a subcritical liquid solvent exhibit an effective attraction at smaller separations and a long ranged weak repulsion, as a consequence of the finite thickness of the solvent vapour density distribution around the solute particles. The solutes, having such a mutual interaction, can aggregate on a length scale of a few nanometres. Our observations show a 'bottom-up' route to the synthesis of a technologically important class of materials, namely, nanostructured thin films where the traditional electrostatic assembly may not be possible [22]. Our predictions are verifiable in real-space experiments of confined suspensions, for instance, a sterically stabilized colloidal suspension added in a non-adsorbing polymer binary mixture solution between glass plates [23].

We thank R Evans, S Dietrich and A A Louis for helpful discussions and the DFG for support within the SFB TR6.

References

[1] Kajimoto O 1999 *Chem. Rev.* **99** 355
[2] Ibanez E *et al* 2003 *J. Agric. Food Chem.* **51** 375
[3] Beysens D and Narayanan T 1999 *J. Stat. Phys.* **95** 997
[4] Galatola P *et al* 2003 *Phys. Rev.* E **67** 031404
[5] Bagchi B and Biswas R 1999 *Adv. Chem. Phys.* **109** 207
[6] Likos C N 2001 *Phys. Rep.* **348** 267
[7] Claesson P M *et al* 1996 *Adv. Colloid Interface Sci.* **67** 119
[8] Bauer C *et al* 2000 *Phys. Rev.* E **62** 5324
[9] Archer A J *et al* 2002 *Europhys. Lett.* **59** 526
Archer A J and Evans R 2003 *J. Chem. Phys.* **118** 9726
M Kinoshita 2001 *Chem. Phys. Lett.* **333** 217
Louis A A *et al* 2002 *Phys. Rev.* E **65** 061407
Qin Y and Fichthorn K A 2003 *J. Chem. Phys.* **119** 9745
Gil T *et al* 1997 *Biophys. J.* **73** 1728
Shinto H *et al* 2002 *J. Chem. Phys.* **116** 9500
Shinto H *et al* 2002 *Langmuir* **18** 4171
Wensink E J W *et al* 2000 *Langmuir* **16** 7392
[10] Greberg H and Patey G N 2001 *J. Chem. Phys.* **114** 7182
[11] S Dietrich 1988 *Phase Transitions and Critical Phenomena* vol 12, ed C Domb and J L Lebowitz (London: Academic) pp 1–128
[12] Dzubiella J and Hansen J P 2004 *J. Chem. Phys.* **121** 5514
[13] Sciortino F *et al* 2004 *Phys. Rev. Lett.* **93** 055701
[14] Stradner A *et al* 2004 *Nature* **432** 492
[15] Merkel M and Löwen H 1996 *Phys. Rev.* E **54** 6623

[4] We note in the simulations the presence of some big clusters (>20 particles) with low probability. The simulations with bigger system size (200 particles) also show the presence of such big clusters. The big clusters may be thought of as associations of smaller clusters due to the low repulsion barrier. The ground state calculations show that such big clusters are energetically less favourable, and hence occur at much lower probability. The Fourier transform of the $g(r)$ data for the larger system size shows the presence of low wavevector peaks, which is consistent with the presence of the clusters.

[16] Allen M P and Tildesley D J 1987 *Computer Simulation of Liquids* (New York: Oxford University Press)
[17] Louis A A *et al* 2002 *Phys. Rev.* E **65** 061407
[18] Mossa S *et al* 2004 *Langmuir* **20** 10756
[19] Claessen P A and Christensen H K 1988 *J. Phys. Chem.* **92** 1650
[20] Brerard D R *et al* 1993 *J. Chem. Phys.* **98** 7236
[21] Bratko D *et al* 2001 *J. Chem. Phys.* **115** 3873
[22] Rotello V (ed) 2004 *Nanoparticles* (New York: Kluwer–Academic)
Zhao Q *et al* 2003 *J. Nano. Res.* **5** 567
[23] Poon W C K 2002 *J. Phys.: Condens. Matter* **14** R859
[24] Karanikas S and Louis A A 2004 *Phys. Rev. Lett.* **93** 248303
Liu J and Luijten E 2004 *Phys. Rev. Lett.* **93** 247802